Chapter 6 Characteristics of the Spin-Glass Transitions Associated with Transverse and Longitudinal Freezing Using Polycrystalline Samples

6.1 Introduction

The study of phase transitions in frustrated magnetic systems is a frontline area of research in condensed matter and material sciences [40,62,358–361,149,334,352–357]. The most commonly investigated source of frustration is frozen-in substitutional disorder leading to a competition between ferromagnetic (FM) and antiferromagnetic (AFM) interactions [57,60,61,362]. Such a competition and randomness in certain situations can prevent the emergence of long-range ordered (LRO) phases and instead give rise to a unique spin-glass state in which the spins are randomly frozen below a frequency (ω) and field (H) dependent peak temperature, usually called as spin-glass freezing temperature (T_f (ω, H)), in the temperature dependence of magnetic susceptibility. Further, the spin dynamics shows critical slowing down and diverges at the spin-glass transition temperature as a result of ergodic symmetry breaking [57,60,61]. This divergence has been taken as a evidence for the thermodynamic nature of the spin-glass transition at T_{SG} [60,61].

Frustration may also arise due to nearest neighbour AFM interactions alone due to the geometry of the lattice [40,62,358–360] for spins arranged on the edge shared triangular (e.g. $YbZnGaO_4$) [355], corner shared triangular or kagome (e.g. $SrSn_2Fe_4O_{11}$, $Cd_2Cu_3(OH)_6(SO_4)24H_2O$, $BaNi_3(OH)_2(VO_4)_2$, $Pr_3Ga_5SiO_{14}$, $Ba_2Sn_2Ga_3ZnCr_7O_{22}$, $SrGa_{12-x}Cr_xO_{19}$) [22,259,363–366], pyrochlore (e.g. $Y_2Mo_2O_7$, $Lu_2Mo_2O_7$, $Tb_2Mo_2O_7$, $A_2Sb_2O_7$ with A=Mn, Co, Ni) [327,329–331,334,367] and spinel (e.g. MAl_2O_4 with M = Co, Fe, & Mn) [337,356] lattices. Such geometrically frustrated systems have evinced enormous attention in recent times as they exhibit exotic spin liquid (quantum as well as

classical) [62,147], spin ice [62,361,368,369] and spin-glass transitions [19,21–23,249,334,370] even in the absence of any frozen-in apparent random substitutional (positional)-disorder (e.g. pyrochlores [327,329–331,334,367], spinels [337,356] and h-$DyMnO_3$ [249]). This is facie quite intriguing as both frustration and randomness have been regarded as the essential ingredients for the occurrence of spin-glass transition [57,60,61,362].

Theoretical calculations seem to suggest that in the absence of any positional-disorder, and hence randomness, the ground state of the geometrically frustrated systems has macroscopic degeneracy with no phase transition down to the absolute zero temperature [340,371,372]. However, it has also been shown that even an infinitesimal random disorder in the few body exchange interactions [332,340], caused by anisotropic exchange interactions due to nearest neighbour bond length variations [330,334,341,342] and/or magnetoelastic strains [332] or dipole-dipole interactions between uncompensated spins or spin clusters with intra-cluster geometrical frustration [341,342,373–375], can lift the degeneracy of the ground state and induce phase transitions to spin liquid [355,367], spin-glass [249,334,355].

In chapter 5, using ac susceptibility data $\chi(\omega, T)$ as a function of temperature (T) and frequency ($\omega = 2\pi f$), we showed that $BaFe_{12}O_{19}$ (BFO) exhibits a series of four spin-glass transitions without any apparent positional disorder due to the dilution of the magnetic sublattice. These transitions were shown to involve successive freezing of transverse and longitudinal spin components of the spins. The observation of the spin-glass transition in BFO without any substitutional disorder and suggests that BFO also belongs to the class of geometrically frustrated magnets like pyrochlores [327,329–331,334,367], spinels [337,356] and $DyMnO_3$ [249]. While the experimental evidence for geometrical frustration in BFO is the subject matter of a later chapter (chapter 8), we

present in this chapter a detailed characterization of the first two spin-glass transitions from the higher temperature side, reported in the previous chapter, using polycrystalline samples. It was possible to put these transitions to additional tests for confirming their spin-glass character, as the signatures of these transitions are much stronger in the polycrystalline samples. Our results mimic the theoretical predictions for conventional disordered Heisenberg systems near the percolation threshold limit [376] even though the source of frustration in BFO is geometry of the lattice [40,357,359,360], as discussed in chapter 8, and not the positional (site)-disorder. Besides confirming the divergence of the spin dynamics at $T_{SG\perp c}$ and $T_{SG//c}$ for the transverse and longitudinal components of the spins, we have also drawn the T-H diagram of BFO using $\chi(\omega, T)$ measurements under different dc magnetic field bias. The T-H diagram reveals that the transverse and longitudinal spin-glass freezing temperatures shift to lower temperatures with increasing magnetic field along the well-known Gabay-Toulouse (G-T) and Almeida-Thouless (A-T) lines, predicted theoretically for disordered Heisenberg systems [64,65,68]. Further, we also present evidence for other characteristics of the spin-glass phase such as non-exponential growth of isothermal remanent magnetization (IRM), aging, rejuvenation and memory effects [69–75,249,377] below the $T_{SG\perp c}$ and $T_{SG//c}$ temperatures.

6.2 Experimental

Polycrystalline BFO was synthesized using solid-state reaction method while single crystals were grown using high-temperature flux method, the details of which are already given in chapter 2. The alternating current (ac) magnetic susceptibility ($\chi(\omega, T)$) measurements on the powder and single-crystalline samples at a fixed frequency with an ac drive field of 3 Oe were carried out using a SQUID-based magnetic property measurement system (MPMS-3, Quantum Design, USA). The $\chi(\omega, T)$ with varying ac

drive fields, frequency, time and aging were measured on powder samples using a physical property measurement system (PPMS, Quantum Design, USA).

6.3 AC susceptibility χ(ω, T, H, t) Studies on $BaFe_{12}O_{19}$

6.3.1 Comparison of χ(ω, T) of Polycrystalline and Single-Crystalline Samples

Fig. 6.1 compares the χ'(ω, T) and χ''(ω, T) plots for the powder and single-crystal samples for measurements carried out at 700 Hz and 745 Hz, respectively, using an ac drive field of 3 Oe. All the four transitions discussed in chapter 5 are revealed in Figs. 6.1(a) and (b), which depict the variation of $\chi'_{//c}$(ω, T), $\chi''_{//c}$(ω, T) and $\chi'_{\perp c}$(ω, T), $\chi''_{\perp c}$(ω, T) with temperature, respectively. Our focus in this chapter are the transitions revealed in χ'(ω, T) around 60 K and 25 K in the $\chi'_{\perp c}$(T) and $\chi'_{//c}$(T) plots. A comparison of the $\chi'_{\perp c}$(T) and $\chi'_{//c}$(T) plots around these two transitions with the χ'(T) plot of the powder sample shown in Fig. 6.1(c) reveals that these two transitions are hidden in a very broad hump with a peak around 65 K in agreement with earlier reports [139].

To resolve the two-transition hidden in the broad hump in the χ'(T) plot of the powder samples, we varied the amplitude of the ac-drive field. The results of such a study carried out at a frequency of 200 Hz on the PPMS set-up are shown in Fig. 6.2(a) for ac drive fields from 3 Oe to 13 Oe at a step of 2 Oe. It is evident from this figure that the broad hump seen in χ'(T) in Fig. 6.1(c) is due to two transitions at temperatures below and above the hump temperature. This is shown more clearly on a magnified scale for the 50 Hz frequency and 13 Oe ac drive field in Fig. 6.2(b). The two peaks around 61 K and 25 K are clearly resolved in this figure for 13 Oe drive field. On the other hand, the same transitions are not well resolved at 50 Hz for the ac drive field of 3 Oe. This can be seen from Fig. 6.2(b) which depicts χ'(T) measured at 50 Hz using ac drive field of 3 Oe and 13 Oe. Thus, we conclude that the higher temperature transition around 61 K in Fig. 6.2 is related to the transverse component of the spins lying in the ab-plane while the lower

temperature transition around 25 K is linked with the longitudinal spin component parallel to the c-axis.

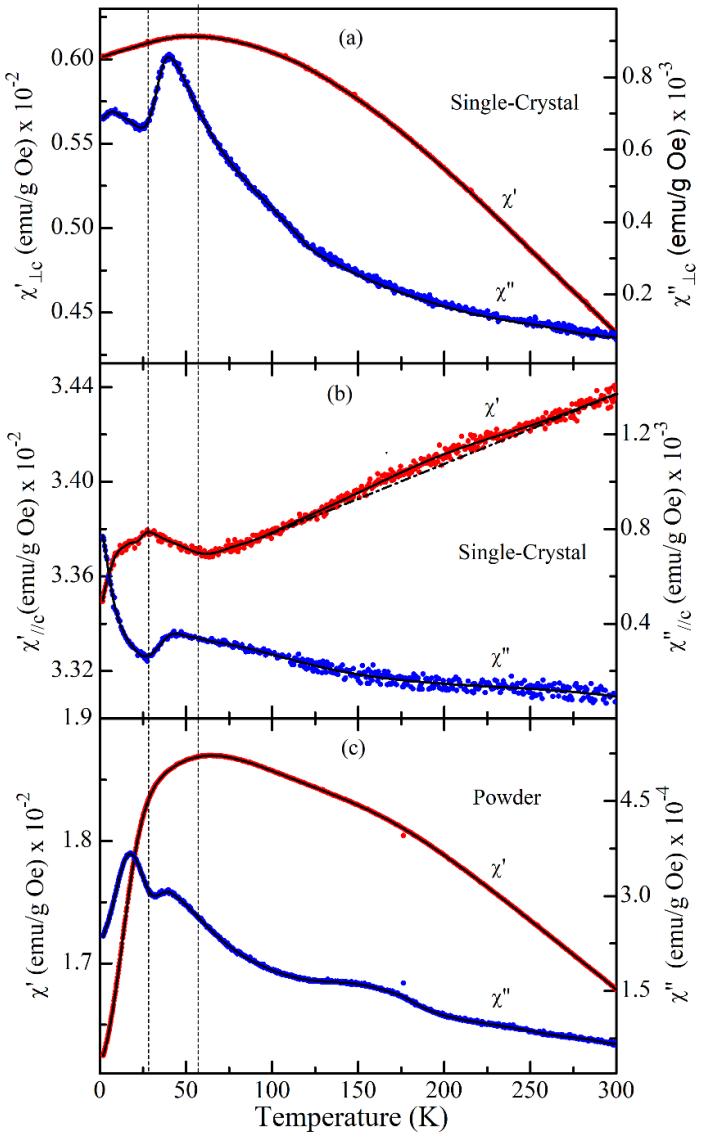

Figure 6.1: Temperature dependence of $\chi'_{//c}$ and $\chi''_{//c}$ measured at 700 Hz with an ac field drive of 3 Oe applied (a) parallel (//) to the c-axis and (b) perpendicular (⊥) to the c-axis of the BFO crystals. This figure has been reproduced from chapter 5. (c) This figure depicts the real χ' and imaginary χ'' parts of ac susceptibility measured at 700 Hz on powder samples at an ac drive field of 3 Oe. The continuous solid line through the data points (filled circles) is guide to the eyes. The dotted vertical lines indicate the first two transitions around 60 K and 25 K in the single-crystal sample.

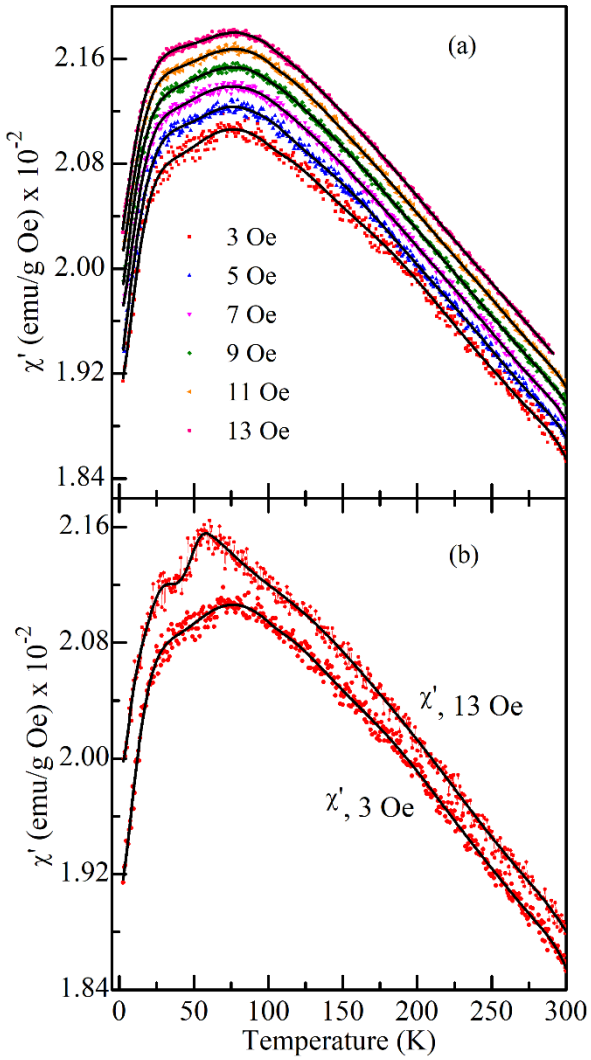

Figure 6.2: (a) The evolution of ac susceptibility measured on powder sample at (a) 200 Hz with different ac drive fields and (b) comparison of ac susceptibility measured at 50 Hz using ac drive field of 3 Oe and 13 Oe. Successive curves in (a) are shifted vertically by 0.0001 emu/gOe for clarity. The continuous solid line through the data points is guide to the eyes.

6.3.2 Confirmation of Ergodicity Breaking for the two Transitions in $BaFe_{12}O_{19}$ Powder

The ac-susceptibility ($\chi'(\omega, T)$) plots of the powder samples of BFO measured at various frequencies using an ac drive field of 13 Oe is shown in Fig. 6.3. It is evident from this figure that the two transition temperatures shift towards higher temperature side with increasing measuring frequency ($\omega = 2\pi f$). A similar frequency-dependent shift of

the high-temperature transition was reported earlier also using $\chi'(\omega, T)$) data on powder samples but the nature of this transition was not analysed [139]. As pointed out in the preceding chapter, such a shift can occur as a result of blocking transition of superparamagnetic (SPM) clusters of spins or spin-glass freezing [57,60,61,244]. The two processes can be distinguished by investigating the temperature dependence of the spin relaxation time ($\tau = 1/\omega$), as mentioned in chapter 5, since SPM blocking follows Arrhenius law (see Equation (5.2) of chapter 5) while spin-glass freezing exhibits critical slowing down of the spin relaxation time. The non-linear nature of the $\ln(\tau)$ vs $1/T_f'$ plot, where T_f' is the peak temperature in $\chi'(T)$ at various frequencies, shown in Figs. 6.4 (a) and (b) for the two transitions rules out the SPM blocking for which this plot should have been straight line, as discussed in chapter 5. For spin-glass freezing, τ shows divergence at a characteristic spin-glass transition temperature T_{SG}' below the frequency-dependent spin-glass freezing temperature $T_f'(\omega)$ as a result of ergodic symmetry breaking [57,60].

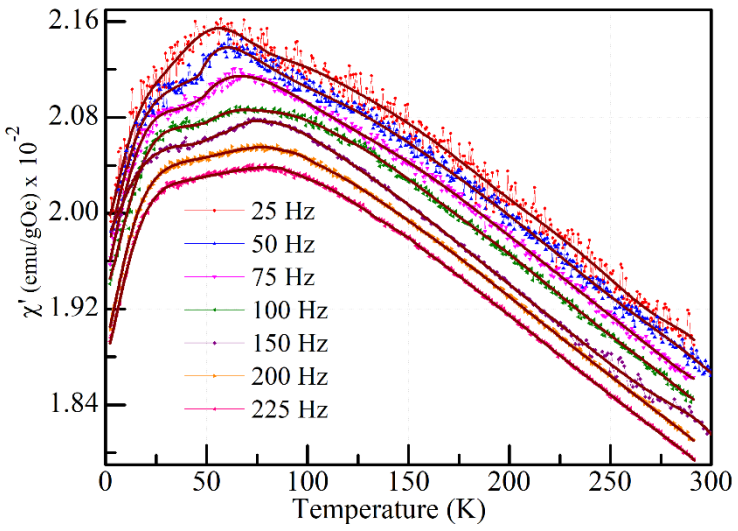

Figure 6.3: Temperature dependence of the real part of ac susceptibility ($\chi'(\omega, T)$) of the powder sample at various frequencies. Successive curves are shifted vertically by 0.00015 emu/gOe for clarity. The solid lines (wine coloured) are guide to the eyes.

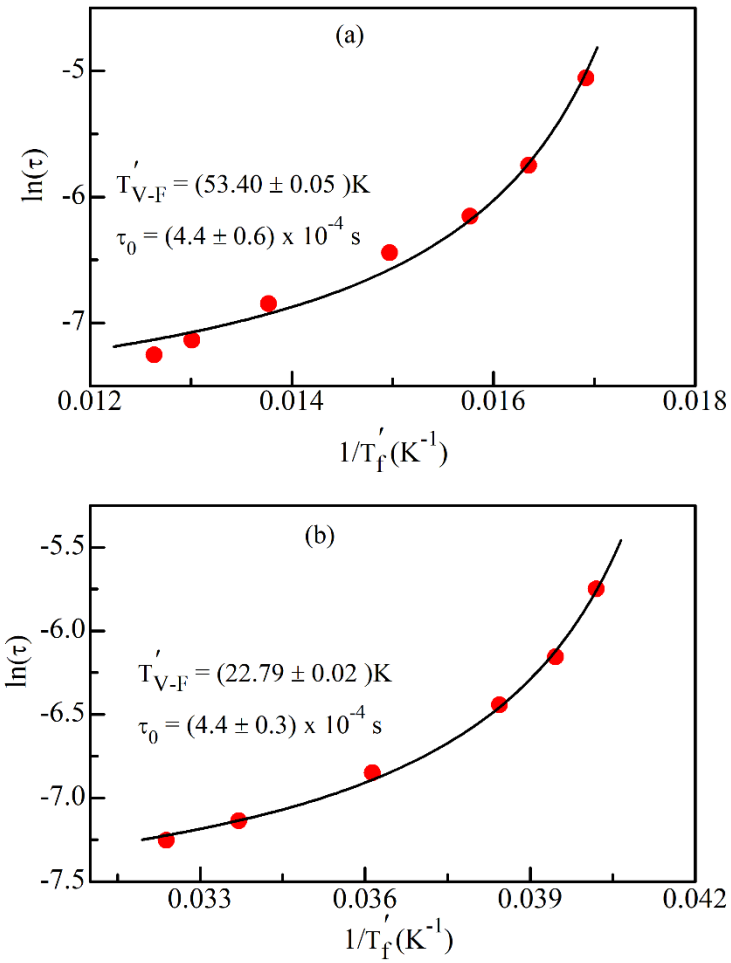

Figure 6.4: The ln(τ) versus $1/T_f'$ plots for the (a) transverse and (b) longitudinal component of the spins. The continuous solid line through the data points is the Vogel-Fulcher fit.

Such a critical dynamics for spin-glasses can be modelled in terms of Vogel-Fulcher law [254] as well as power-law behaviour [57,60,378] based on scaling theories [57,60], as already discussed in chapter 5 (see Equations (5.3) and (5.4) of chapter 5). The least-squares fits for the ln(τ) versus $1/T_f'$ plot shown in Figs. 6.4(a) and (b) using Vogel-Fulcher law are shown by continuous lines through the data points in the same figure. The fitting parameters obtained after the least-squares fit are $T'_{V-F\perp c}$ = (53.40 ± 0.04) K, $\tau_{0\perp c}$ = (4.4 ± 0.06) x 10^{-4} s, $E_{a\perp c}$ = (1.3 ± 0.05) meV with a goodness of fit (GoF) = 0.985 for the transverse (⊥c) freezing. The corresponding parameters for the longitudinal (//c) freezing:

$T'_{V-F//c}$ = (22.79 ± 0.02) K and $\tau_{0//c}$ = (4.4 ± 0.3) x 10^{-4} s, $E_{a//c}$ = (0.35 ± 0.006) meV with a GoF = 0.996 for the higher and lower temperature transitions, respectively. To obtain the critical spin-glass transition temperature (T_{SG}) using power-law, we followed the steps discussed in section 5.3.1 of chapter 5. The optimization curves (i.e., variance (σ) vs T'_{SG}) to locate the T'_{SG} value precisely for the two transitions are shown in Figs. 6.5(a) and (b). These figures reveal minimum at $T'_{SG\perp c}$ = (57.325 ± 0.025) K and $T'_{SG//c}$ = (24.39 ± 0.04) K corresponding to the spin-glass transition temperatures for the transverse and longitudinal components of the spins, respectively. Using these T'_{SG} values, the least-squares fits for the ln(τ) versus ln(T'_f - T'_{SG})/T'_{SG} plot are shown by continuous lines through the data points in Figs. 6.6(a) and (b). The fitting parameters for the power-law are: $z\nu_{\perp c}$ = (0.86 ± 0.02) and $\tau_{0\perp c}$ = (3.2 ± 0.02) x 10^{-4} s with GoF = 0.997 and $z\nu_{//c}$ = (0.58 ± 0.04) and $\tau_{0//c}$ = (3.3 ± 0.06) x 10^{-4} s with a GoF =0.999 for the transverse and longitudinal freezing of the spins components, respectively. A comparison of the GoF values for the Vogel-Fulcher and power-law fits suggests that the power-law fits are better. The excellent fits seen in Figs. 6.6(a) and (b) confirm the spin-glass character of

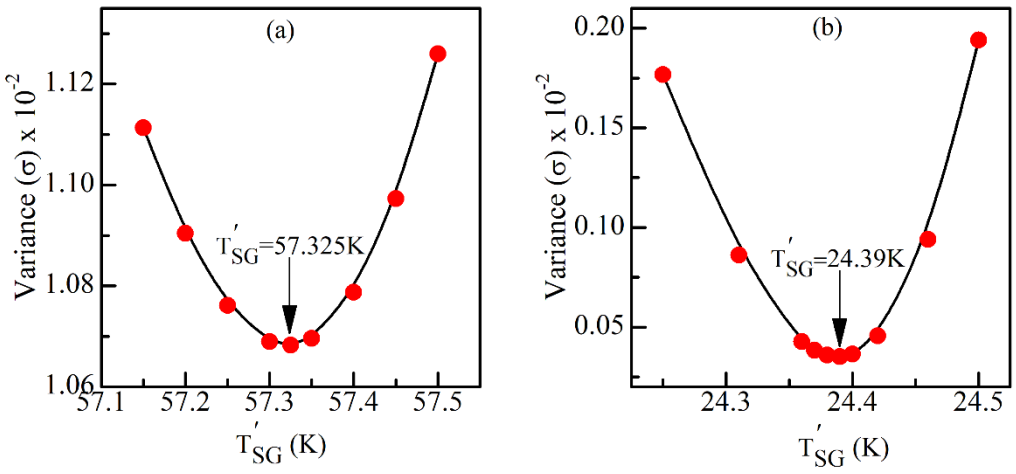

Figure 6.5: Optimization of the spin-glass transition temperature (T'_{SG}) for (a) transverse and (b) longitudinal freezing.

the two transitions.

The large value of the attempt relaxation time (τ_0) of the order of 10^{-4} sec for both the transitions obtained by Vogel-Fulcher and power-law fits suggest cluster spin-glass behaviour [301,310], as τ_0 for the atomic glasses is known to be much smaller (10^{-12} to 10^{-13} s) [57,60,307,379,380]. Presence of local clusters of spins has been reported in several ordered compounds with frozen-in geometrical frustration by diffuse neutron scattering and small- angle neutron scattering (SANS) [257,381] and has formed the basis

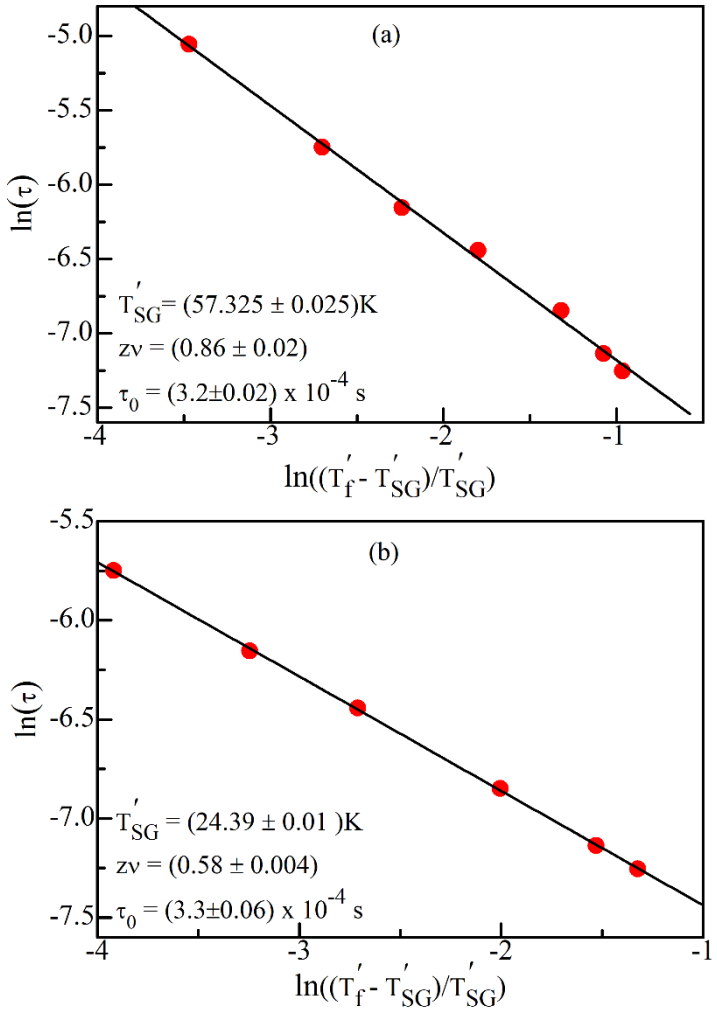

Figure 6.6: The $\ln(\tau)$ *vs* $\ln(T_f' - T_{SG}')/T_{SG}'$ plots for the freezing of the (a) transverse and (b) longitudinal components of the spins. The continuous line through the data points is the power-law fit.

of several theoretical models of spin-glass transition in ordered compounds [332,340–342,345–347]. We believe that the large value of τ_0 in BFO is due to the involvement of such spin clusters in the spin-glass freezing.

6.3.3 Evidence for the Gabay-Toulouse (G-T) and Almeida-Thouless (A-T) lines

Stability of the spin-glass phase under dc field has been quite controversial as many workers believed that the spin-glass phase is unstable the under dc field [74,264,382–384] Using mean-field approximation, de Almeida and Thouless demonstrated theoretically for the Ising glasses that replica symmetry breaking occurs even in the presence of the magnetic field [64]. It was shown that the spin-glass freezing temperature (T_f) decreases with increasing field (H) and T_f(H) shifts along a characteristic Almeida-Thouless (A-T) line whose extrapolation to H = 0 gives T_f(H = 0). For low fields, they showed that this field dependent shift of T_f(H) follows the following functional dependence:

$$H^2 = A\left(1 - \frac{T_f(H)}{T_f(0)}\right)^3, \qquad \text{…….(6.1)}$$

where $T_f(0)$ is similar to T_{SG} in the limit of $H \rightarrow 0$ and A is a constant. For the disordered Heisenberg systems also, Gabay and Toulouse [65] showed that spin-glass phase is stable under dc field but there are two transition lines in the T-H plane corresponding to the breaking of the ergodic and replica symmetries, respectively. The field (H) dependence of the Gabay-Toulouse (G-T) line [65,68] in the T-H plane can be expressed as:

$$H^2 = B\left(1 - \frac{T_f(H)}{T_f(0)}\right), \qquad \text{…….(6.2)}$$

where B is a constant. Sherrington and his coworkers [68] later on demonstrated that both the ergodic and replica symmetries are broken simultaneously at the first transition itself. However, this transition crosses over to another transition, which may not be strictly a thermodynamic phase transition, at a lower temperature giving rise to the G-T and A-T

lines in the T-H plane reported earlier by Gabay and Toulouse [68]. Sherrington and his coworkers predicted a theoretical T-H phase diagram where small but positive single-ion anisotropy would lead to the appearance of A-T line first followed by G-T line at lower temperatures. The situation is inversed for small but negative single-ion anisotropy with G-T line preceding the A-T line in the T-H plane [66]. Bray et al., later on showed that apart from the weak single-ion anisotropy, the A-T and G-T lines can appear successively as a result of exchange anisotropy also, even if it is not sufficiently weak [236].

Experimentally, in spin-glass systems (canonical spin-glass as well as cluster spin-glasses) the A-T and G-T lines were drawn in the T-H plane using either the freezing temperature $T_f(H)$ from the ZFC plot [75,249,305,385,386] or the irreversibility temperature $T_{irr}(H)$ [75,306,386–388] between the ZFC and FC magnetization curves. Further, the $T_f(H)$ vs H plot has been generated using the peak temperature in the ac $\chi'(T)$ plot measured under different dc bias fields at a fixed frequency [389]. We have used the peak temperature T_f' at a frequency of 200 Hz using 13 Oe ac drive field under different dc bias fields to study the T-H phase diagram. The two spin-glass freezing temperatures $T_f'(200\ Hz)$ shift to the lower temperature side under dc bias field (H), as can be seen from Fig. 6.7 which depicts $\chi'(T)$ plot under different dc bias fields. These shifts are phenomenologically similar to those observed in the conventional disordered systems. The least-squares fits to the $T_f(200\ Hz)$ *versus* H plots for the two transitions shown in Fig. 6.8 give m = (2.0 ± 0.004) and (0.65 ± 0.001) for the spin-glass transition involving transverse and longitudinal components of the spins. These exponents match very well with the exponents for the G-T and A-T lines in the conventional spin glasses [74,386,390–392]. It is interesting to note that $3d^5Fe^{3+}$ spins at the 12k Wyckoff site has got negative single-ion anisotropy whereas its sign is positive for $3d^5Fe^{3+}$ spins at other Wyckoff sites. This suggests that the $3d^5Fe^{3+}$ spins at the 12k site are most likely

candidate for canting and giving rise to the components // and ⊥ to the c-axis. It is interesting to note that for negative single-ion anisotropy, the theoretical T-H diagram for conventional disordered Heisenberg systems, the G-T line precedes the A-T line as we lower the temperature in excellent agreement with the experimentally observed T-H diagram of BFO shown in Fig. 6.8.

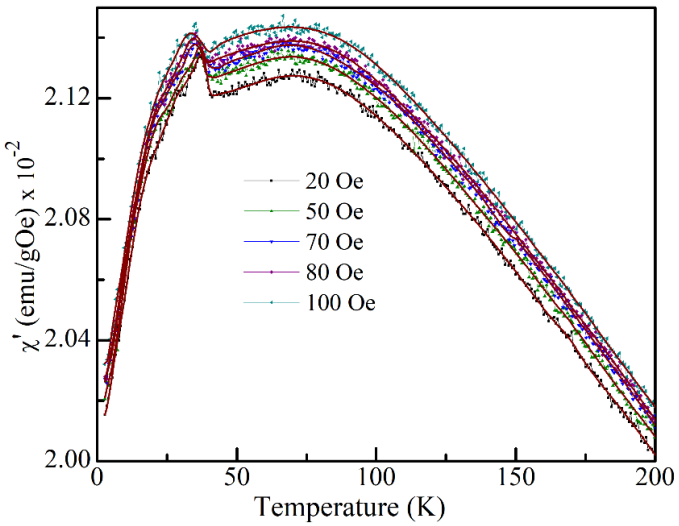

Figure 6.7: The χ'(ω=200Hz, T) plot for powder sample under different dc biasing magnetic field. The solid lines through the data points are guide to the eyes.

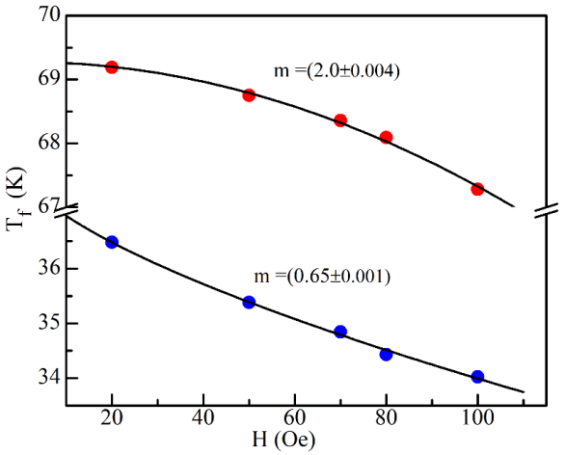

Figure 6.8: The T-H diagram showing the Gabay-Toulouse (G-T) with m = (2.0 ± 0.04) and de Almeida-Thouless (A-T) with m = (0.65 ± 0.001) lines. The continuous line through the data points in the T-H plane is the least-squares fit to the Equation (6.1) and (6.2).

6.3.4 Evidence for the None-Exponential Relaxation: Isothermal Remanent Magnetization (IRM)

The exact functional form for aging and long-time relaxation has been quite controversial. Sherrington and Kirkpatrick (S-K) have proposed a power-law type dependence on time for the thermoremanent magnetization (TRM) in the spin-glass state [326]. There are a few experimental reports [393–396] that confirm the power-law type relaxation. Besides power-law, a logarithmic dependence of TRM on time in cluster spin glasses has also been used [397–399] whose genesis lies in the Neel theory of superparamagnetism [400]. However, capturing logarithmic dependence using a finite interval of time of measurement has been questioned [250]. For strongly interacting clusters in glasses including spin-glasses, Palmer et al. [251] have given a generalized theory based on the hierarchically constrained dynamics. According to these workers, the time dependence of TRM in spin glasses should follow a stretched exponential functional behaviour as a result of distribution of relaxation time in the spin-glass state [251]. Most workers have reported such a stretched exponential functional [74,249,306,394,401–403] even though the debate on the theoretical models of relaxation in spin glasses continues to debate even in the current literature [74,249,405,306,394–396,401–404].

The nature of relaxation of the magnetization can be studied either by investigating the decay of the remanent magnetization of a dc field cooled sample after switching of the field or by studying the growth of the remanent magnetization of a zero-field cooled sample on the application of dc filed as a function of time. These protocols are called thermoremanent magnetization (TRM) and isothermal remanent magnetization (IRM) studies, respectively [73,251]. It is important to note that both the TRM and IRM relaxations have been studied using either dc magnetization or ac susceptibility data at a fixed temperature below T_{SG} as a function of time [69–74].

In order to investigate the relaxation of ac susceptibility χ' in the spin-glass phases of BFO using the powder samples, we quenched the sample from 370 K to 40 K ($< T'_{SG\perp c}$) in zero magnetic field and allowed it to age for a wait time of t_w = 60 seconds. After the elapse of time t_w, we applied dc magnetic field of 50 Oe and measured the growth of χ' as a function of time at 200 Hz with an ac drive field of 13 Oe. The same protocol was used to measure the evolution of χ' as a function of time at 10 K *(*$< T'_{SG//c}$*)*. Figs. 6.9(a) and (b) depict the evolution of $\chi'(\omega = 200$ Hz) of BFO as a function of time

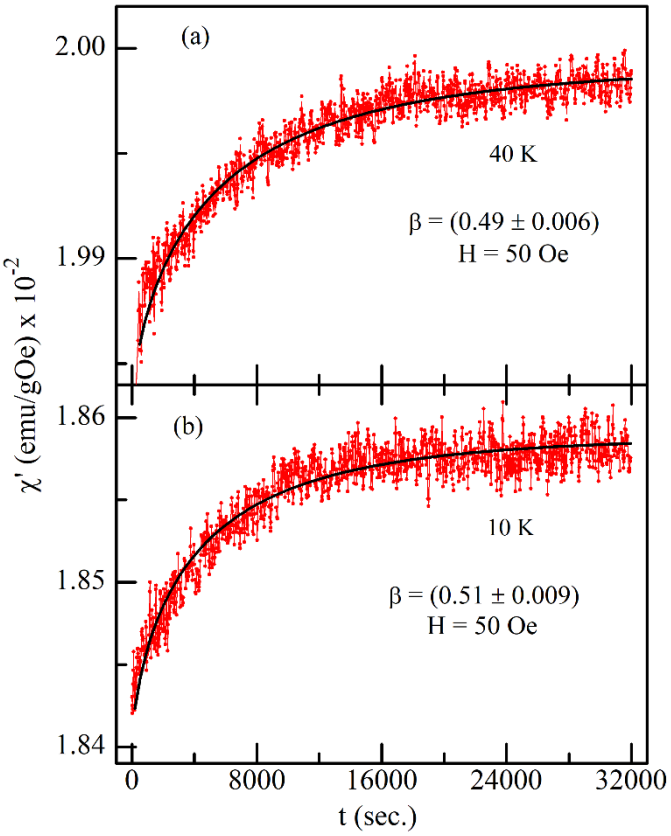

Figure 6.9: Evolution of iso-thermoremanent ac susceptibility $\chi'(\omega = 200$Hz) with time at (a) 40 K and (b) 10 K under 50 Oe dc biasing field. The solid lines (black coloured) through the data points in (a) and (b) are Kohlrausch-Williams-Watt (KWW) stretched exponential equation fits.

under dc field bias of 50 Oe at 40 K (< $T'_{SG\perp c}$) and 10 K (< $T'_{SG//c}$) on the zero-field cooled powder samples.

We fitted the Kohlrausch-Williams-Watt (KWW) stretched exponential function [250,406] to the two χ'(t) data in Fig. 6.9:

$$\chi'(t) = \chi'_0 + \chi'_g \exp\{-\left(\frac{t}{\tau}\right)^{\beta}\}, \qquad \text{.....(6.3)}$$

where τ is the characteristic relaxation time and the parameter β is a measure of departure from Debye type exponential function β = 1. The least-squares fits to the relaxation of IRM using the above KWW stretched exponential function gives an excellent fit with χ'_0 = (0.013 ± 3 x10^{-7}) emu/gOe and (0.0199 ± 5 x10^{-7}) emu/gOe, χ'_g = - (1.57 ± 0.01) x 10^{-4} emu/gOe and - (1.64 ± 0.03) x 10^{-4} emu/gOe, τ = (7829 ± 8) sec and (6008 ± 8) sec and β = (0.65 ± 0.003) and (0.66 ± 0.004), respectively, at 40 K and 10 K, respectively. The value of β so obtained at 40 K and 10 K reveals non-exponential behaviour in contrast to β = 1 for the ordered systems. In conventional spin glasses, values of β in the range 0 < β < 1 has been reported as signature of slow non-exponential relaxation [57,60,248–251] due to presence of metastable states with different energy barriers. Our β values lies in the range reported for the conventional spin glasses and in disordered systems [57,60,248–251] and confirms slow non-exponential relaxation of the IRM below the two spin glass transition temperatures.

6.3.5 Study of Aging, Rejuvenation and Memory Effect in $BaFe_{12}O_{19}$

Spin-glass phase is known to exhibit characteristic aging, rejuvenation and memory effects below T_{SG} [72,73,407]. This has been explained in terms of the hierarchical [70] and droplet [408] model of the spin-glass state. In the hierarchical model [70], spin-glass state is assumed to consist of many metastable states with finite energy barriers between them at any temperature below T_{SG}. These states further divide into more number of metastable states with decreasing temperature. During the waiting

time (t_w) at any temperature T_1 below T_{SG}, various metastable states in the system gradually relax into the nearby lower energy states on decreasing the temperature. On increasing the temperature from say T_1 to T_2 ($T_1 < T_2 < T_{SG}$) the system "rejuvenates" back to the previous state as per this model suggesting that the system remembers the previous history. This effect is often called memory effect [70,409]. The aging and memory effects are regarded as characteristics of the conventional spin glasses and cluster glasses as they provide evidence for the evolution of spins from one set of metastable free-energy minima to another with time and temperature [69,70,377].

To probe the memory effects in our samples below $T'_{SG\perp c}$ and $T'_{SG//c}$, we used the following protocol [72,73,407]: the sample was initially cooled down to T_1 = 40 K (< $T'_{SG\perp c}$) under zero magnetic field and $\chi'(t)$ was recorded at 200 Hz with an ac drive field of 13 Oe in the presence of a dc biasing field of H = 50 Oe for 8 hours [segment "gh" in Fig. 6.10(a)]. After 8 hours, the sample was quenched to a lower temperature T_2 = 35 K, such that T_1-T_2 = 5 K), in the presence of the same biasing field and $\chi'(t)$ was again recorded over 6 hours at the same frequency and same ac drive field [segment "ij" in Fig. 6.10(a)]. Finally, the sample was heated back to 40 K and then $\chi'(t)$ was recorded for 6 hours again at the same frequency, ac drive field and the dc biasing field [segment "kl" in Fig. 6.10(a)]. It is evident from Fig. 6.10(a) that the relaxation process during the segment "kl" is simply a continuation of the process during the segment "gh". This behavior of $\chi'(t)$ suggests that the state of the system before cooling to T_2 = 35 K is recovered when the sample is heated back to the initial temperature i.e. T_1 = 40 K. Using the same protocol with ΔT = 5 K, we have confirmed memory effects at 10 K (< $T'_{SG//c}$) below the second spin-glass phase transition temperature also (see figure 6.10(b)). The observation of both non-exponential relaxation and memory effects below $T'_{SG\perp c}$ and $T'_{SG//c}$ confirms

the presence of metastable states in the spin-glass phases of BFO have phenomenological similarities with the conventional spin glasses [57,60,61,362].

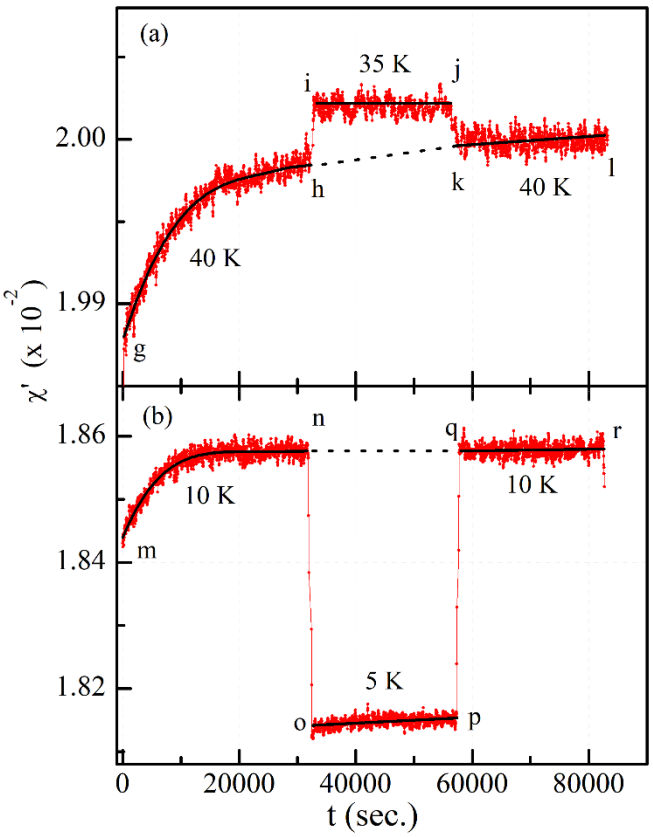

Figure 6.10: Evolution of isothermal remanent ac susceptibility $\chi'(\omega=200Hz)$ with time at (a) 40K and (b) 10K under 50 Oe dc biasing field measured with intermediate quenching to 35K and 5K, respectively. The solid lines (black coloured) though the data points in (a) and (b) are guide to the eyes.

6.4 Conclusions

(1). Successive freezing of transverse and longitudinal spin components with spin-glass transition temperatures $T'_{SG\perp c} \sim 57.3$ K and $T'_{SG//c} \sim 24.3$ K was confirmed using ac susceptibility studies on polycrystalline samples and comparing them with the single-crystal data of chapter 5.

(2). Stability of the spin-glass phase was investigated under dc bias field. A T-H diagram showing the presence of G-T and A-T lines was constructed using $\chi'(\omega = 200Hz)$ measurements under varying dc field bias. These results using powder samples confirm that the transverse spin component freezes first at $T'_{SG\perp c}$ and follows the G-T line in the T-H plane. Subsequently, the longitudinal spin component also freezes at $T'_{SG//c}$ and follows the A-T line in the T-H plane. Both are surprisingly in excellent agreement with theoretically predicted T-H diagram for the negative single-ion anisotropy in disordered Heisenberg systems [66].

(3). Characteristic non-exponential relaxation, memory and rejuvenation effects were observed below the $T'_{SG\perp c}$ and $T'_{SG//c}$. Observation of these effects suggests the presence of metastable states below the $T'_{SG\perp c}$ and $T'_{SG//c}$ in analogy with conventional disordered systems.